THE ASTROPHYSICAL JOURNAL, 216:462–478, 1977 September 1

HIGH-RESOLUTION POLARIZATION OBSERVATIONS INSIDE SPECTRAL LINES OF MAGNETIC Ap STARS. I. INSTRUMENTATION AND OBSERVATIONS OF β CORONAE BOREALIS

ERMANNO F. BORRA
Département de Physique, Université Laval, Québec, and Observatoire Astronomique du Québec
AND
ARTHUR H. VAUGHAN
Hale Observatories, Carnegie Institution of Washington, California Institute of Technology
Received 1976 November 8; accepted 1977 February 23

ABSTRACT

We have constructed a coudé photon-counting polarimeter capable of attaining (with a Fabry-Perot interferometer) a high resolution. A description of the instrument is given, with a discussion of various sources of systematic error in the polarimetry. Observations of linear and circular polarization in the spectrum of the Ap star β Coronae Borealis, throughout the magnetic cycle, are obtained across an Fe II and a Sm II line at a resolution of 0.086 Å. Inferences are drawn regarding the magnetic geometry of the star: the geometry appears to be devoid of any symmetry but can probably still be approximated by a decentered dipole model. The longitudinal magnetic curve of the star is derived from the available data.

Subject headings: instruments — polarization — stars: individual — stars: magnetic — Zeeman effect

I. INTRODUCTION

The measurement of stellar magnetic fields is generally made through the Zeeman effect (Babcock 1960). Although in strong fields and sharp lines the separation of the σ components can be large enough to be measured in high-dispersion spectra of some stars (HD 215441, 53 Cam, β CrB, etc.), usually it is small compared with the width of the spectral lines. It therefore cannot usually be measured directly.

By the use of a quarter-wave plate and calcite beam splitter to produce simultaneously two parallel spectra of a star, one in left circular polarized light, the other in right circular polarized light, the separation of the two circular polarized components of a spectral line in a magnetic star can be measured spectroscopically. By analogy with the longitudinal Zeeman effect, the average stellar longitudinal component of the magnetic field can thus be obtained. However, this method is limited to sharp-lined stars, and even in the best case the standard error is of the order of a couple of hundred gauss (Preston 1969*a*).

A photoelectric method capable of detecting much weaker fields was devised by Hale (1933) and Kiepenheuer (1953) and perfected by Babcock (1953) for the observation of sunspots. The instrument measures, photoelectrically, the circular polarization in a fixed point of one wing (or two points on opposite wings) of a spectral line. The longitudinal field is derived directly from the polarization signal. To eliminate scintillation noise, the signal is rapidly modulated by a rotating quarter-wave plate. Babcock replaced the wave plate by an electro-optic crystal of ammonium dihydrogen phosphate (ADP). Alternating the direction of a strong electric field across the faces of the crystal produces the necessary alternation between positive and negative quarter-wave retardations. This improvement avoids mechanical modulation of the light at the same frequency as the modulation of the signal.

In stellar astronomy, this magnetograph technique has been applied to the detection of magnetic fields by Babcock (1955) and more recently by Angel and Landstreet (1970), Severny (1970), Borra and Landstreet (1973), Borra, Landstreet, and Vaughan (1973), and others.

The purpose of the present work is to obtain photoelectric polarization scans across the spectral lines of several bright magnetic Ap stars. The shape of those Zeeman signatures should be of considerable use in determining the geometry of the stellar magnetic fields. This first paper will discuss the instrumentation used and present polarization and intensity scans for the magnetic Ap star β Coronae Borealis.

II. INSTRUMENTATION

The observations were obtained by photon counting with the coudé scanner of the 2.5 m Mount Wilson telescope equipped with a Fabry-Perot interferometer (Vaughan and Zirin 1968). The interferometer used has a half-power bandwidth of about 0.086 Å. To this instrument we added a Pockels cell photon-counting polarimeter that will be described in the present paper. The polarimeter is located in front of the entrance slit of the spectrograph to minimize instrumental polarization effects. The layout of the instrument is shown in Figure 1.

The principal element of the polarimeter is a Lasermetrics 402A KD*P electro-optic modulator (EOM). When a proper electric field is applied to the entrance faces of the EOM, it acts as a quarter-wave plate, converting incident circularly polarized light into linearly polarized light. A Glan-Thompson prism, used as a linear polarizer, transmits the linearly polarized light whose electric vector is parallel to its transmission axis and extinguishes light polarized with the electric vector perpendicular to its transmission axis. The transmission axis of the Glan-Thompson prism is oriented at 45° with respect to the fast and slow axes of the EOM. Because changing the sign of the electric field applied to the EOM changes the sign of its retardation, either left or right circularly polarized light incident upon the EOM is transmitted into the spectrometer, depending on the sign of the electric field applied to the EOM. The great advantage of this technique is that the net circular polarization is detected as a difference in intensity measured with only one phototube between half-cycles of electric polarity (and retardation) reversals, rather than as a difference in intensity between two different detectors. If the electric field of the EOM is alternated rapidly enough, the polarimetry is insensitive to drifts in tube sensitivity, changes in intensity due to variable atmospheric extinction, scintillation, guiding errors, etc. In practice we reverse the polarity one thousand times per second. Notice also that the left circular and right circular components enter the spectrograph as light linearly polarized with the same orientation of the electric vector, as defined by the Glan-Thompson prism. They also enter the spectrograph along the same optical path. We are thus measuring two beams identical in all but their intensity, which gives the net circular polarization. In particular, because the two beams are linearly polarized in the same direction (given by the Glan-Thompson prism), we do not have to worry about the fact that the grating transmits different orientations of linear polarization with different efficiencies. In our arrangement, the Glan-Thompson prism (and therefore the EOM) has been oriented to maximize the efficiency of the spectrograph; but the polarization properties of the latter have no effect on our stellar polarization measurements because the polarization is analyzed before the light enters the spectrograph.

In practice, the light incident on the EOM does not have the same state of polarization as the starlight entering the telescope, primarily because of the phase shift and polarization introduced by the oblique reflection of the light from the aluminized coudé flat mirror of the telescope. The phase shift, which depends on the declination (and other incidental factors, such as wavelength), can be calibrated experimentally. Its effect can then be essentially eliminated by means of a variable retardation plate (a Babinet-Soleil compensator) that rotates with hour angle to follow the rotation of the optical fast and slow axes of the flat.

Two photomultiplier tubes are used. One is located so it measures intensity (photon counting) in the scanned narrow bandpass of the Fabry-Perot interferometer. The other measures the intensity (also photon counting) in a pair of fixed bands, each 25 Å wide, one on each side of the scanned passband. Pulses from these two detector channels are fed to an array of four digital counters (two for the interferometer phototube and two for the continuum phototube), after passing through a gating and timing control unit, as illustrated schematically in Figure 1. The control unit sets and times the alternating electric field applied to the EOM with a high-voltage pulser so as to produce alternating plus and minus quarter-wave retardation at a set frequency (0.5 kHz). Thus each detector receives light that was polarized in one sense or the opposite sense according to the sign of the applied field, its signal being gated to the appropriate counter (A or B for the interferometer, C or D for the continuum) for each state of polarization. The control unit, which contains the gating circuitry, and the high-voltage pulser driving the EOM are timed so that the gates are opened only when the EOM phase shift has risen to its definitive value; transients during the switching are thus not detected. A crystal clock controls the switching to ensure that the gates are open for equal times.

If A and B are the counts recorded at the end of an integration on the two counters for the line profile and C and D are the same for the continuum, then

$$P_1(\lambda) = (A - B)/(A + B) \tag{1}$$

is the fractional polarization in the spectral line channel, and

$$P_2 = (C - D)/(C + D) \tag{2}$$

is the apparent fractional polarization in the fixed continuum reference channel of the spectrometer. At the same time,

$$(A + B)/(C + D) = I(\lambda) \tag{3}$$

gives the line profile which is then normalized to 1 on the continuum. A nonzero value of P_2 is attributed to the polarization of the light in the continuum of the star if such polarization is present, plus various instrumental effects that will be discussed in the following sections. Thus the observed spectral line polarization will be given by

$$P(\lambda) = P_1(\lambda) - P_2\,. \tag{4}$$

Our apparatus also can be used to measure linear polarization. This can be done by introducing a quarter-wave plate just ahead of the EOM (converting linearly polarized light into circular, which is then measured in the manner already described). Alternatively, the electric field applied to the EOM could be set to alternate between zero and

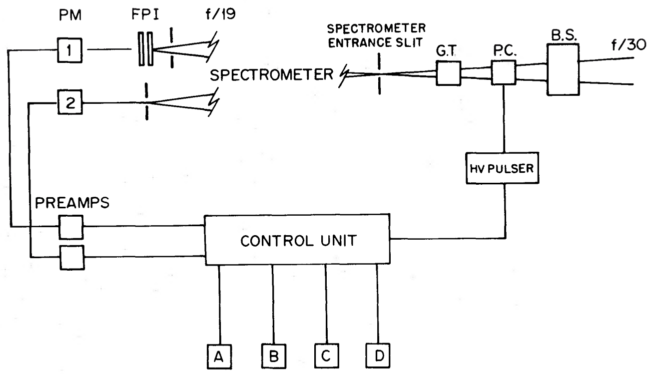

FIG. 1.—Block diagram showing the apparatus

a half-wave retardation at the chopping frequency; but the first method was actually used. To be able to determine the total linear polarization and the orientation of the electric vector in the plane of the sky, one must be able to vary the azimuth of the quarter-wave plate.

III. SOURCES OF ERROR IN THE MEASUREMENT OF CIRCULAR POLARIZATION

Because of the high switching frequency of the EOM, any noise introduced by seeing scintillation, variable atmospheric extinction, drifts in detector sensitivity, and guiding errors can be ignored. Sky background is negligible. The stars discussed in this and following papers are sufficiently bright that detector background is a small enough fraction of the observed signal that it can either be ignored or corrected reliably. Thus photon shot noise remains the principal source of random noise in our observations. In the case of β CrB ($m_v = 3.8$), an integration time of around 10 minutes per point was sufficient to accumulate enough counts for a photon noise level of 0.5% (percentual polarization).

Systematic errors can be encountered as the result of differential absorption and phase shift on reflection from the coudé flat, improper thickness adjustment or orientation of the Babinet-Soleil compensator, incorrect voltages applied to the EOM resulting in non-quarter-wave retardation, asymmetrical modulation of the EOM, improper alignment between the Glan-Thompson and the EOM, or improper tilt of various elements in the polarimeter. In addition, the convergence of the f/31 coudé beam of the telescope introduces some error in the discrimination of polarized light in our apparatus. Errors of timing, producing unequal integration cycles in the gating electronics, could also introduce errors in our measurements, but, in practice, this is a negligible source of error. In any event, the residual timing error appears as a spurious polarization in the continuum channel and is thus automatically removed during the data reduction.

The effect of those errors will be cross-talk among the Stokes parameters, depolarization and thus failure to measure the percentage of polarization actually present, and apparent instrumental polarization. These effects can be studied with the help of Müller calculus (Shurcliff 1962).

A reflection by a metallic mirror introduces linear polarization and a phase shift, both dependent upon wavelength and angle of incidence (Borra 1976). The first two reflections from the primary and secondary mirrors are essentially normal; the polarization introduced is thus very small and the two nearly half-wave phase shifts cancel each other to a very good approximation. The third flat mirror of the 2.5 m coudé has an angle of incidence $\varphi = \frac{1}{2}(90° + \delta)$ where δ is the declination. Figure 3 shows the linear polarization measured for this mirror at various declinations and at a wavelength of 4520 Å. The electric vector is contained in the s-plane (perpendicular to the plane of incidence), and therefore it rotates with hour angle with respect to the entrance slit. This instrumental polarization is taken into account in the reduction of our data.

The phase shift introduced by the flat mirror is compensated at the telescope with a Babinet-Soleil compensator. The compensation curve has been determined by measuring, at several declinations, a light source, diffuser, and polaroid placed in front of the flat. Because the fast optical axis of the flat is contained in the plane of incidence (p-plane) and thus rotates with hour angle with respect to the analyzer, the compensator has to be motor-driven to follow it. The calibration of the compensator is shown in Figure 2. The wavelength is 4520 Å. Note that the compensation applied is such as to advance the phase shift to half a wave, rather than to cancel it. This changes the sign of polarization and is taken into account during data reduction.

Because the starlight suffers only one oblique reflection, we do not have a significant instrumental circular polarization from the telescope optics. However, some of the linear polarization introduced by the flat is converted into circular by cross-talk caused by the analyzing optics. This spurious circular polarization is usually small ($<0.2\%$) and varies very slowly with time. The main source of this time variation is probably the compensator's motor, which does not turn at quite the exact sidereal rate; and the time variation is also due to the fact that the

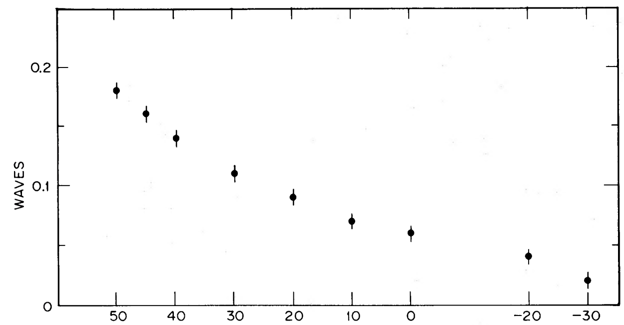

FIG. 2.—Compensation curve for the flat mirror of the 100 inch (2.54 m) coudé. The compensation is expressed in fractional wavelength and has been determined experimentally at 4520 Å.

electric vector rotates with respect to the fixed analyzing optics. The instrumental circular polarization is measured in the two wide bands in the continuum and is removed during data reduction.

A first depolarization of the incoming stellar signal occurs because the flat mirror acts as a partial polarizer. This effect of the flat as a partial polarizer on the incoming Stokes vector $[I] = [I, Q, U, V]$ representing the incident starlight can be described by the matrix equation (Shurcliff 1962; Borra 1976):

$$\frac{1}{2}\begin{vmatrix} k_s + k_p & -k_s + k_p & 0 & 0 \\ -k_s + k_p & k_s + k_p & 0 & 0 \\ 0 & 0 & 2(k_s k_p)^{1/2} & 0 \\ 0 & 0 & 0 & 2(k_s k_p)^{1/2} \end{vmatrix} \times \begin{vmatrix} I \\ Q \\ U \\ V \end{vmatrix} = \begin{vmatrix} I' \\ Q' \\ U' \\ V' \end{vmatrix} \tag{5}$$

where $[I'] = [I', Q', U', V']$ is the Stokes vector after the reflection. The coefficients k_s and k_p are the coefficients of reflection in the planes perpendicular (s) and parallel (p) to the plane of incidence, which is chosen as the reference direction. We can write the individual Stokes parameters as

$$I' = \tfrac{1}{2}[(k_s + k_p)I + (-k_s + k_p)Q]\,, \tag{6}$$

$$Q' = \tfrac{1}{2}[-k_s + k_p]I + (k_s + k_p)Q]\,, \tag{7}$$

$$U' = (k_s k_p)^{1/2}U\,, \tag{8}$$

$$V' = (k_s k_p)^{1/2}V\,. \tag{9}$$

Renormalizing to $I' = 1$, and because in our case both Q and $k_p - k_s$ are small, we have to a very good approximation that

$$Q' = (-k_s + k_p)/(k_s + k_p)I + Q\,, \tag{10}$$

$$U' = (k_s k_p)^{1/2}U/\tfrac{1}{2}(k_s + k_p)I\,, \tag{11}$$

$$V' = (k_s k_p)^{1/2}/\tfrac{1}{2}(k_s + k_p)I\,. \tag{12}$$

To see the importance of this depolarization, let us consider the worst case, at a declination of 45°. This is about as far north as it is possible to work at the coudé of the 2.5 m telescope. Taking $k_s = 0.90$ as a reasonable value for an aluminized mirror, we find, from the observed instrumental linear polarization (Fig. 3) at 45° declination, that $k_p = 0.77$, and therefore that $V' = 0.997V$. We can see that this depolarization can be safely ignored. At lower declinations the depolarization is even smaller. This depolarization comes from the same effect discussed by Preston and Pyper (1965).

We now consider the importance of the depolarization and cross-talk that arise from the introduction of a wave plate having azimuth ρ and a small phase shift Δ. This will model the effects caused by misadjustments of the compensator, by the beam convergence, etc. We can describe this with the equation (Shurcliff 1962; Borra 1976)

$$\begin{vmatrix} 1 & 0 & 0 & 0 \\ 0 & D^2 + G^2 - E^2 & 2\,DE & -2\,EG \\ 0 & 2\,DE & -D^2 + G^2 + E^2 & 2\,DG \\ 0 & 2\,EG & -2\,DG & 2\,G^2 - 1 \end{vmatrix} \times \begin{vmatrix} I \\ Q \\ U \\ V \end{vmatrix} = \begin{vmatrix} I' \\ Q' \\ U' \\ V' \end{vmatrix}, \tag{13}$$

where $D = \cos 2\rho \sin \Delta/2$, $E = \sin 2\rho \sin \Delta/2$, and $G = \cos \Delta/2$. The angle ρ is the azimuth of the fast axis with

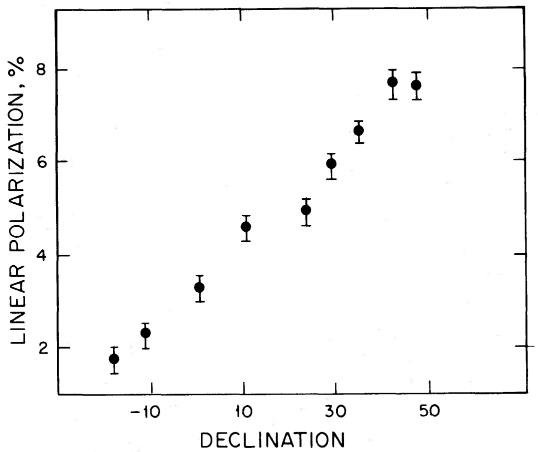

FIG. 3.—Instrumental linear polarization of the 100 inch (2.54 m) coudé. The polarization is expressed in percents and has been determined experimentally at 4520 Å.

respect to the reference direction. Because we chose this direction to lie in the plane of incidence, $\rho = 0$, and therefore $E = 0$ and $D = \sin \Delta/2$. Thus

$$V' = U \sin \Delta + V \cos \Delta \,, \tag{14}$$

and for small Δ,

$$V' = U\Delta + V(1 - \Delta^2/2) \,. \tag{15}$$

The cross-talk depends on Δ in the first order, and the depolarization is the second on Δ. We estimate errors in the compensation (barring a grosser human error) to be less than 0.005 λ. This introduces about a very tolerable 3% cross-talk and a negligible depolarization. In a similar fashion, it can be shown that an error in the voltage necessary to give a $\lambda/4$ retardation decreases V in the second order of the retardation error and does not give any cross-talk, and that if the retardation does not exactly reverse from one half-cycle to the next, this will introduce cross-talk in the first order.

From this discussion we can see that, barring gross errors, the depolarization is negligible but the cross-talk is more critical. We must therefore exercise great care in minimizing the cross-talk by making careful adjustments, and if possible removing what remains from our data. During each setup, and occasionally throughout a run, the cross-talk in the analyzing optics is checked by observing a light source through polaroids. If the cross-talk is more than a couple of percents, the alignment is redone. The magnitude of the total cross-talk of the system was also checked by inserting a light source diffuser and polaroid sheet in front of the (compensated) flat mirror and then observing the spurious circular polarization. The cross-talk was found to be $\sim$3%. We thus expect it to be of this order of magnitude during our actual observations.

The cross-talk will convert some of the interstellar linear polarization into circular. This is removed, along with the instrumental polarization, by observing the continuum with the second photomultiplier. The only instance where unremoved cross-talk could still be present in our data is whenever there is intrinsic linear polarization inside the spectral line different from the polarization of the continuum. This will be the case if the transverse Zeeman effect is important. For sufficiently small fields (< 1000 gauss) the longitudinal Zeeman effect is far more important than the traverse. However, because the circular polarization is roughly proportional to $H_e dI/d\lambda$ while the linear is proportional to $H_e{}^2 d^2I/d\lambda^2$ (Borra 1972), the linear can become comparable to the circular for fields greater than 1000 gauss. The relative importance of the two actually depends on the line profile $I(\lambda)$ and the field geometry.

IV. SOURCES OF ERROR IN THE MEASUREMENT OF LINEAR POLARIZATION

As already mentioned, the linear polarization is measured by adding a quarter-wave plate in front of the EOM. Linear polarization at 45° to the optical axes of the quarter-wave plate is transformed into circular, which is then measured by the polarimeter. The reference direction defining the Q vector is the one running north-south, and the U vector is measured positive in the north-west quadrant. To measure U, which is at 45° to the compensator axes, we simply add a quarter-wave retardation to the thickness of the compensator. To measure Q, we add, behind the compensator, a quarter-wave plate whose axes are at 45° to the axes of the compensator. Instrumental linear polarization contributes uniquely to Q, as shown by equation (7) and Figure 3. In practice, because of various misalignments, instrumental polarization contributes to U as well. In both Q and U, this instrumental effect, as well as any interstellar linear polarization that may be present, is measured by the continuum photomultiplier and subtracted during data reduction.

We shall now, as we did for the circular polarization, consider the depolarization and cross-talk introduced by the system.

Equation (7) shows that Q' differs from Q only by the instrumental polarization which is removed during the data reduction. Equation (8) shows that the relation between U' and U is the same as that between V' and V. We can thus conclude that the depolarization due to the flat acting as a partial polarizer is also negligible.

We now consider the depolarization and cross-talk caused by a phase shift Δ. From equation (13), with $\rho = 0°$, we have $E = 0.0$ and $D = \sin \frac{1}{2}\Delta$, $G = \cos \Delta/2$. Hence,

$$Q' = (\sin^2 \Delta/2 + \cos^2 \Delta/2) = Q\,. \tag{16}$$

Thus, Q' is not affected, but this occurs because of the particular reference direction chosen. The depolarization and cross-talk show up in U', which is given by

$$U' = (1 - \Delta^2/2)U + V\Delta\,. \tag{17}$$

We thus see that, for small errors in the compensation, the depolarization is negligible, while the cross-talk from circular to linear depends on the error in the first order.

Because the quarter-wave plate transforms the linear into circular, which is then measured by the polarimeter, the effects of depolarization and cross-talk in the optics are the same as the ones discussed previously for V. For small Δ we will have a negligible depolarization and some cross-talk ($\sim 2\%$).

The cross-talk is a more serious problem in the measurement of the transverse Zeeman effect because the circular polarization is usually more important than the linear. In our observations, the cross-talk is much more important for Q than U. This comes about because U is measured by adding a $\lambda/4$ to the compensator; this has an error of about 0.005 λ. The parameter Q is measured by adding a mica plate, which does not quite give a $\lambda/4$ retardation at 4520 Å. The actual retardation is measured at $0.23 \pm 0.005\ \lambda$. This introduces a cross-talk $\sim 13\%$, to which one must add (or subtract) the 2% cross-talk in the rest of the system. Thus we could have as much as 15% contamination of the Q by V. It is necessary to know $V(\lambda)$ across the line to correct for it. This correction has been taken into account in the discussion of the transverse Zeeman effect in β CrB by Borra and Vaughan (1976).

V. OBSERVATIONS OF β CORONAE BOREALIS

a) *The Star*

The star β CrB was discovered to be magnetic by Babcock (1958). The average longitudinal magnetic field H_e, measured photographically, varies between approximately +1000 and −800 gauss in a period of 18.487 days (Preston and Sturch 1967). Although the magnetic variations are periodic, Preston and Sturch found some evidence for a secular variation (time scale ~ 10 years) of the south polarity extremum. Confirmation of this variation was claimed by Severny (1970) but not by Wolff and Bonsack (1972). Borra and Dworetsky (1973) have also presented arguments against the secular variation.

The average surface field of the star (H_s) is strong enough to resolve, in conventional spectrograms, some favorable Zeeman patterns (Preston 1969*b*). A knowledge of the H_s curve enables one to test specific models for the magnetic geometry of this star. This has allowed Wolff and Wolff (1970) to conclude that the geometry is such that one pole is stronger than the other. They found that the geometry could be approximately represented by a decentered dipole model (Landstreet 1970). However, they also found indications of departures from this type of geometry, in that the assumption of cylindrical symmetry appears to be inconsistent with the shape of the H_e curve and an observed phase shift between the H_e and H_s curves.

b) *Observations of the Circular Polarization*

The observations were made principally using the λ4520.2 line of Fe II. Although there are lines with larger *z*-factors and simpler Zeeman structure, this line was chosen because it is present in all Ap stars and is unblended and strong, and therefore less subject to spectral changes caused by nonuniform distribution of the elements over the stellar surface. The main disadvantages are that its strength and complicated Zeeman structure (4 π components and 8 σ components) make modeling difficult. Occasionally we also observed the nearby weak line Sm II λ4519.6.

The circular polarization and intensity profiles during the 1973 and 1974 observing season are displayed in Figures 4, 5, and 6. Each scan is identified by the magnetic phase at the midpoint of observation obtained from the ephemeris 2434217.5 + 18.487E (Preston and Sturch 1967). When two separate scans have been taken consecutively on the same night, they have been plotted in the same figure with different symbols. The circular polarization and intensity (normalized to one at the continuum) are sampled at 0.086 Å discrete intervals.

The circular polarization V is expressed in percent, and the line profile is plotted directly underneath it. The convention used is such that a positive longitudinal field as defined by Babcock (1962) gives a positive polarization on the blue wing and a negative polarization on the red wing of the line. The error bar size (± one standard deviation) associated with every single polarization observation of the scan is shown in the upper right-hand corner of each scan; it usually is $\pm 0.5\%$. The standard deviations are computed assuming that photon noise is the only random error. Extensive experience with this type of polarimeter both at the coudé and Cassegrain foci shows

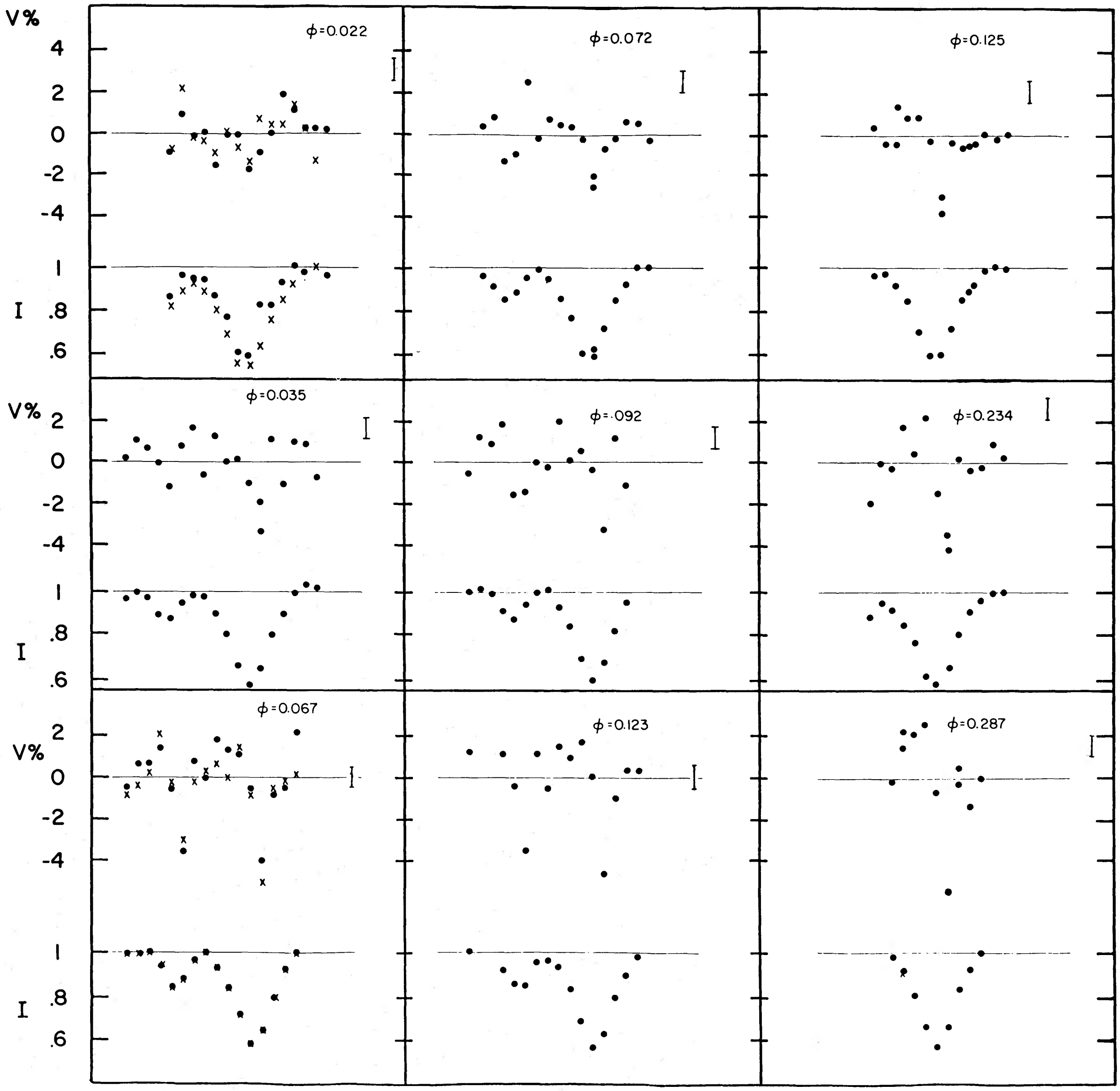

FIG. 4.—The circular polarization and line profiles obtained are shown. The error bars accompanying each polarization scan are equal to two standard deviations ($\pm\sigma$). Wavelength increases to the right.

that this is very nearly the case. One will be convinced by inspecting the figures and comparing two scans taken on the same night, or on different nights but nearly the same phase.

The Zeeman signatures in Figures 4, 5, and 6 contain much information about the magnetic geometry of the star. A detailed analysis by means of the modeling approach proposed by Borra, Landstreet, and Vaughan (1973) is in progress. However, there are some general conclusions about this geometry that we can infer from an inspection of the scans. Throughout the following discussion we will make the implicit assumption that the λ4520.2 line is unblended. Hiltner (1945) published a line identification list for β CrB. From this list we see that the line does not suffer from blends. The nearest line to the shortward is the Sm II line. There is only a negligible overlapping between the far wings of our line and the Sm II line. The nearest line to the longward is the Cr I 4521.14 line, too far to cause blending. Moreover, our profiles do not show obvious asymmetries which indicate blending. The fact that at least at some phases (0.4 to 0.85) the Zeeman signatures appear symmetrical also adds to our confidence. The magnetic extrema of β CrB occur at approximately (Preston and Sturch 1967) phases 0.3 and 0.8. If the magnetic geometry of the star has cylindrical symmetry in the equatorial plane (with a polarity change), like a centered

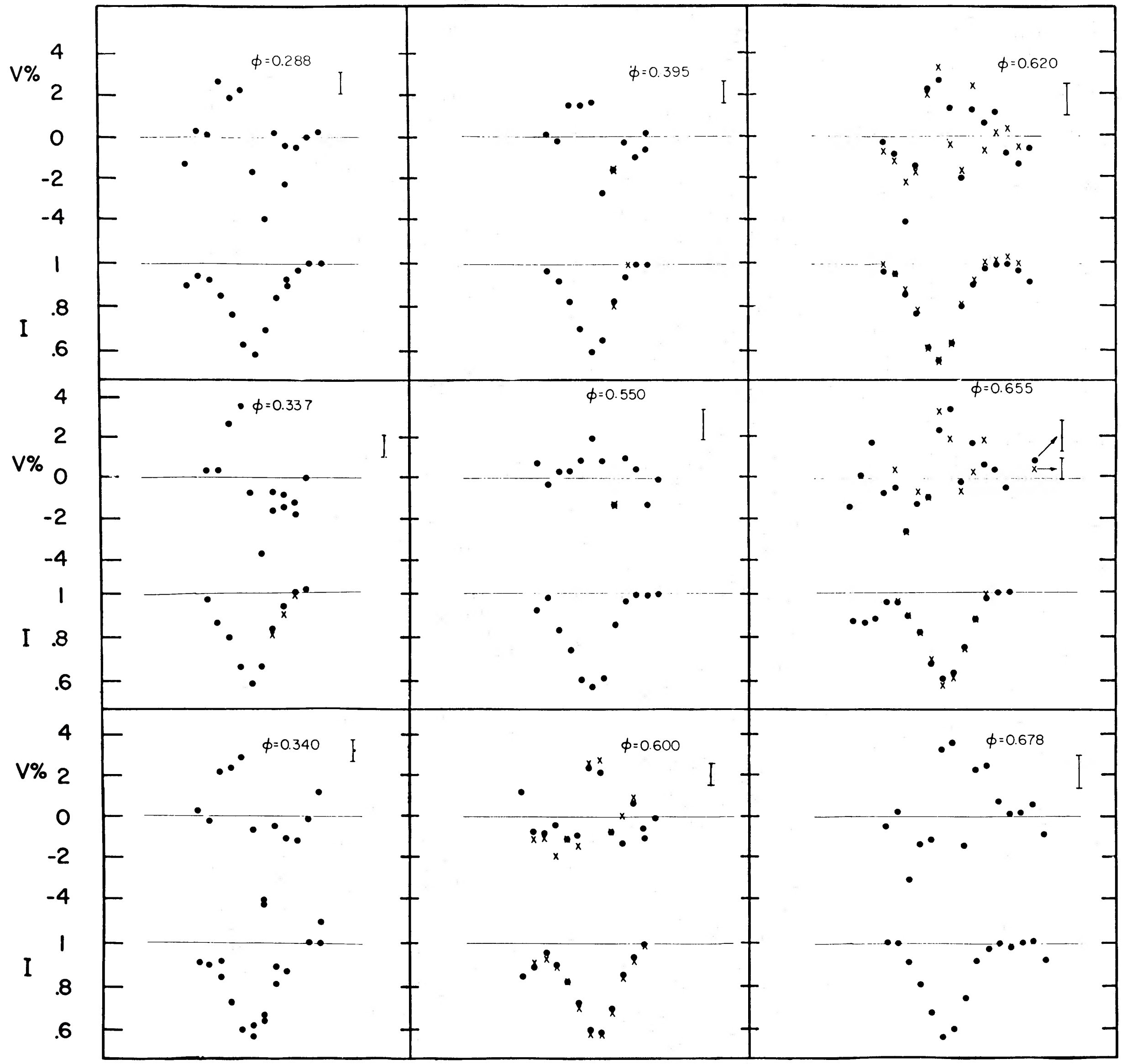

FIG. 5.—Same as Fig. 4

dipolar field, the Zeeman signatures near phase 0.3 should have nearly the same shape (with the signs changed) as those near phase 0.8, because H_e reverses almost symmetrically. We can see that this does not happen. Near phase 0.3 the Zeeman signatures are not quite S-shaped, indicating some crossover. It is only near phase 0.4 that the Zeeman signature has the simple S-shape of a nearly cylindrically symmetric field distribution. We can also see that near positive extremum, the maxima of polarization occur near the line center. This indicates that the regions which have positive polarity have weak fields. Near the phase of negative extremum, the V maxima occur near the wings. This indicates that the regions of negative polarity have a stronger field. This is what one would expect from an asymmetric field distribution such as the decentered dipole.

If the field geometry had cylindrical symmetry, the crossover Zeeman signatures, at phases equally distant from an extremum, should be mirror images of each other, with a sign change. Our scans show that this is not the case. We conclude that the field is not cylindrically symmetric and thus deviates from a simple decentered dipole geometry. For about a third of our scans we also have observed the Sm II line. Our resolution and sampling are clearly insufficient to fully resolve the structure of this weak and narrower line. The Zeeman signatures of the Sm II are compatible with those of Fe II, indicating much the same magnetic field.

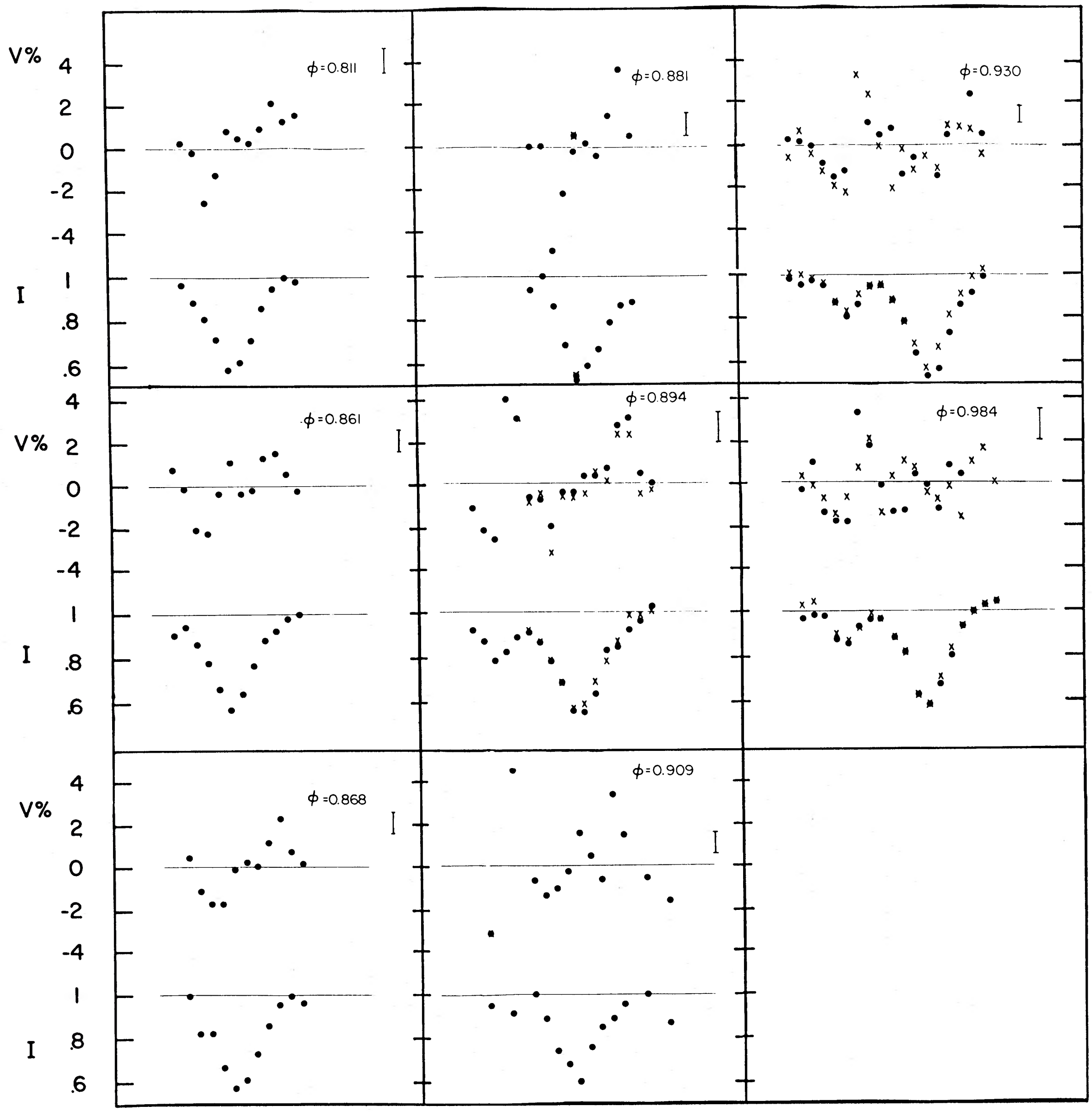

FIG. 6.—Same as Fig. 4

c) *The Longitudinal Magnetic Field*

A measure of the longitudinal field averaged over the visible disk of the star, H_e, can be obtained by determining the separation $2\ \Delta\lambda$ between the spectral lines seen in left and right circularly polarized light. H_e is then given by the relation

$$H_e = 2.14 \times 10^{12}(\Delta\lambda/\lambda^2 z)\,, \tag{18}$$

where z is a factor that depends upon the Zeeman structure of the line (Babcock 1962) and the units used are angstrom and gauss. We adopt $z = 1.5$ for the 4520.2 line as given by *LS* coupling and confirmed by photographic observations of several magnetic stars. The longitudinal field obtained from equation (18) is a good measure of the true H_e, even during crossover (Borra 1974*a*, *b*, and unpublished computations) if the geometry is reasonably uniform (such as a dipole or a moderately decentered dipole). It is shown in the Appendix that the separation $\Delta\lambda$ is given by

$$\Delta\lambda = \int \lambda V_c(\lambda) d\lambda \Big/ \int r_I(\lambda) d\lambda\,, \tag{19}$$

where $r_I(\lambda)$ is the residual intensity and $V_c(\lambda)$ is the fractional circular polarization expressed in units of the continuum. Note that in the Zeeman effect the condition

$$\int V_c(\lambda)d\lambda = 0 \tag{20}$$

obtains.

An important source of error comes about because every numerical method we can use to compute the integrals in equation (19) utilizes a fitting procedure. Because of insufficient sampling, the uncertainty in the fitting is large. Most of the error arises in the evaluation of $\int \lambda V_c(\lambda)d\lambda$. The accuracy can be substantially improved with a correction making use of equation (20). Let us consider that our observations are fitted by the function

$$f(\lambda) = V_c(\lambda) + \delta(\lambda)\,, \tag{21}$$

where $\delta(\lambda)$ is a function describing the error in the fitting. If $\delta(\lambda)$ does not change sign in the interval of integration, the generalized first mean theorem allows us to write

$$\int \lambda V_c(\lambda)d\lambda = \int \lambda f(\lambda)d\lambda - \bar{\lambda} \int \delta(\lambda)d\lambda\,, \tag{22}$$

where $\bar{\lambda}$ is a value of λ in the interval of integration. In practice we expect $\delta(\lambda)$ to change sign in the interval of integration, and the correction equation (22) provided is no longer rigorously valid. It is valid, however, in each interval, if we split the integration into several intervals in which $\delta(\lambda)$ does not change sign. We find an approximate value of

$$\int \delta(\lambda)d\lambda$$

by integrating numerically

$$\int f(\lambda)d\lambda \approx \int \delta(\lambda)d\lambda$$

from our data. This comes about from equation (20). We then take $\bar{\lambda}$ to be the wavelength at the midpoint of the interval of integration. The correction thus computed and applied with equation (22) is obviously not exact, but does reduce significantly the scatter in the values of H_e without correction. That the correction is imperfect becomes evident if one computes (with correction) H_e from the same data but using different integration techniques (trapezoidal, Simpson's first and second rules). The values of H_e thus obtained can vary by as much as 200 gauss even though the identical data are used.

As an alternative method of obtaining H_e from our data, it can be shown that, for fields giving a splitting smaller than the half-width of the line and in the absence of crossover, the circular polarization at one point of the profile is given to first order by the approximate formula

$$V = 4.6710^{-13} z H_e \lambda^2 (1/I(\lambda)) dI(\lambda)/d\lambda\,, \tag{23}$$

where V is the fractional polarization and $I(\lambda)$ the intensity profile of the line. We can obtain H_e by least-squares fitting the straight line of equation (23) to the observed $V(\lambda)$ as a function of $1/I\; dI/d\lambda$. During crossover, polarization is present that is not represented by equation (23). Nevertheless, if a longitudinal field component H_e is present, it will be detected by fitting equation (23) to our data. Thus we can use this procedure to analyze our data for β CrB at all phases.

In Table 1 we list the values of H_e obtained from the first method (eq. [19]) and the trapezoidal rule. The same data are plotted in Figure 7, along with the photographic H_e curve from Preston and Sturch (1967). We estimated the standard error associated with a typical observation by hand-fitting a smooth curve through the data and obtaining the deviations from it. The standard error is 195 gauss.

The values of H_e obtained with the second method are listed in Table 2 and plotted in Figure 8 along with the photographic H_e curve. The standard deviation associated with a typical observation has also been computed from a hand-fitted curve. The standard error is 115 gauss.

If we compare the data in Figures 7 and 8 with the photographic H_e curve, we see that there is a general agreement in the amplitude and shapes of the photoelectric and photographic observations, although there are systematic differences. The photographic curve has a somewhat greater positive extremum, while its negative extremum agrees well with the data in Figure 7 but is a bit greater in Figure 8. Another feature of both figures is that the photoelectric data do not show evidence of the anharmonicity of the photographic curve. This anharmonicity is present in the photographic H_e curves of many Ap stars and has been an obstacle to our understanding of magnetic geometries (Wolff and Wolff 1970; Preston 1971). Borra (1974*b*) has argued on theoretical grounds that the anharmonicity is not real but is rather an artifact of the photographic technique. This has been confirmed observationally by Borra and Landstreet (1977). On the basis of Figures 7 and 8 it would appear that the same is true again for β CrB.

TABLE 1

Longitudinal Fields Obtained with the Integral Equation

JD 2440000+	Phase	H_e
2222.78	0.022	−467
2222.78	0.022	−288
1871.77	0.035	−29
1779.86	0.064	+280
1779.98	0.070	+361
2223.70	0.072	+60
1872.82	0.092	+303
1780.96	0.123	+313
2224.69	0.125	+260
2226.69	0.234	+117
1783.98	0.287	+648
2227.69	0.288	+636
1784.92	0.337	+747
2228.65	0.340	+900
1785.99	0.395	+507
1899.77	0.550	+218
1900.71	0.600	−26
1900.71	0.600	−384
2196.85	0.620	−500
2196.90	0.622	−670
1901.71	0.655	−695
1901.71	0.655	−425
2197.91	0.678	−999
2181.90	0.811	−734
2182.83	0.861	−474
2145.99	0.868	−687
1757.99	0.881	−880
2091.01	0.894	−706
2091.01	0.894	−760
1740.03	0.909	−657
1869.78	0.928	−421
1869.87	0.932	−305
1870.80	0.982	−223
1870.87	0.986	−199

TABLE 2

Longitudinal Fields Obtained with the Differential Equation

JD 2440000+	Phase	H_e
2222.78	0.022	−48
2222.78	0.022	−142
1871.77	0.035	+112
1779.86	0.064	+373
1779.98	0.070	+387
2223.70	0.072	+135
1872.82	0.092	+247
1780.96	0.123	+401
2224.69	0.125	+252
2226.69	0.234	+374
1783.98	0.287	+651
2227.69	0.288	+648
1784.92	0.337	+701
2228.65	0.340	+648
1785.99	0.395	+444
1899.77	0.550	+46
1900.71	0.600	+25
1900.71	0.600	−160
2196.85	0.620	−70
2196.90	0.622	−170
1901.71	0.655	−420
1901.71	0.655	−174
2197.91	0.678	−337
2181.90	0.811	−274
2182.83	0.861	−271
2145.99	0.868	−340
1757.99	0.881	−582
2091.01	0.894	−335
2091.01	0.894	...
1740.03	0.909	−413
1869.78	0.928	−175
1869.87	0.932	−112
1870.80	0.980	+152
1870.87	0.986	−93

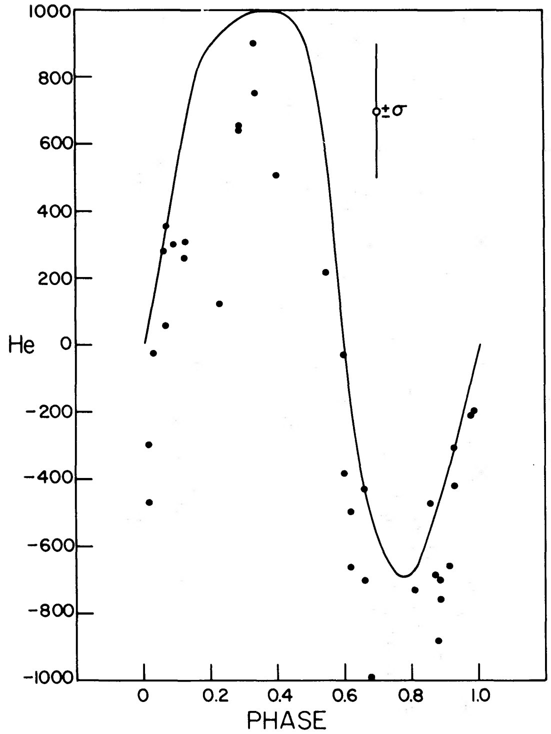

FIG. 7

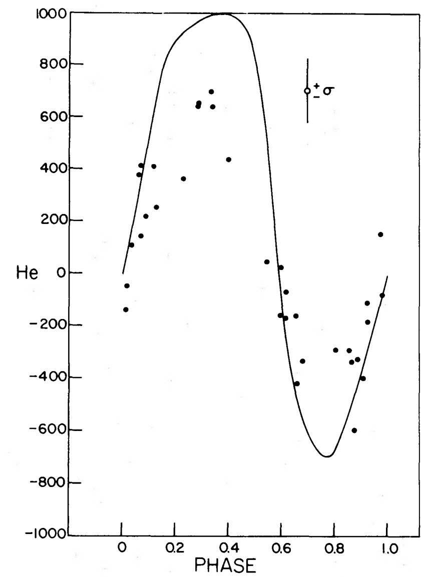

FIG. 8

FIG. 7.—Longitudinal magnetic curve obtained with the integral equation. The continuous line is a hand-fit through the longitudinal fields determined photographically by Preston and Sturch (1967).

FIG. 8.—Longitudinal magnetic curve obtained with the differential equation. The continuous line is a hand-fit through the longitudinal fields determined photographically by Preston and Sturch (1967).

However, we cannot be as definite as Borra and Landstreet were for 53 Cam and α^2 CVn; the random errors in our figures are large. Moreover, the fact that the two figures disagree shows that one or both of them contain systematic errors that vary throughout the cycle. This is just the essence of the criticisms Borra has expressed regarding the photographic observations.

If we compare the two sets of H_e values in Figures 7 and 8, we see that the two agree reasonably well except at negative polarity, where the two extrema differ by almost a factor of 2. This is not surprising, given the peculiar shape of the Zeeman signatures at south polarity, which do not show the S-shaped form given by the first derivative of the line profile (eq. [23]). It is also not surprising that we encounter difficulty at this part of the magnetic cycle if we remember the controversy about the behavior of the negative extremum of β CrB. The agreement at north polarity is better because the profiles are more nearly S-shaped.

Notice that even though the standard error associated with Figure 8 is smaller than the one in Figure 7, this does not necessarily mean that the second method is superior. The second method also tends to give smaller fields. When we compare the signal-to-noise ratios, we see that they are comparable. We shall await the reduction of our data on other stars (in preparation) before commenting on the relative merits of the two methods.

d) *Observations of the Transverse Zeeman Effect*

The linear polarization has also been measured across the λ4520.2 Fe II line. Figures 9, 10, and 11 show the scans obtained (Q and U expressed in percents). These figures have been plotted in a fashion similar to that used for the circular polarization. The cross-talk in Q has not been removed from the data displayed. One can, however, do so easily by adding 0.13 $V(\lambda)$, using the appropriate V scans in Figures 4 to 6.

We will not discuss these scans, as this has already been done by Borra and Vaughan (1976). They can be used, along with the observations of the circular polarization, in modeling the geometry of β CrB.

VI. CONCLUSIONS

We have constructed and used a photon-counting coudé polarimeter interfaced with the coudé scanner and Fabry-Perot interferometer of the Mount Wilson 2.5 m telescope. The instrument provides us with the wavelength

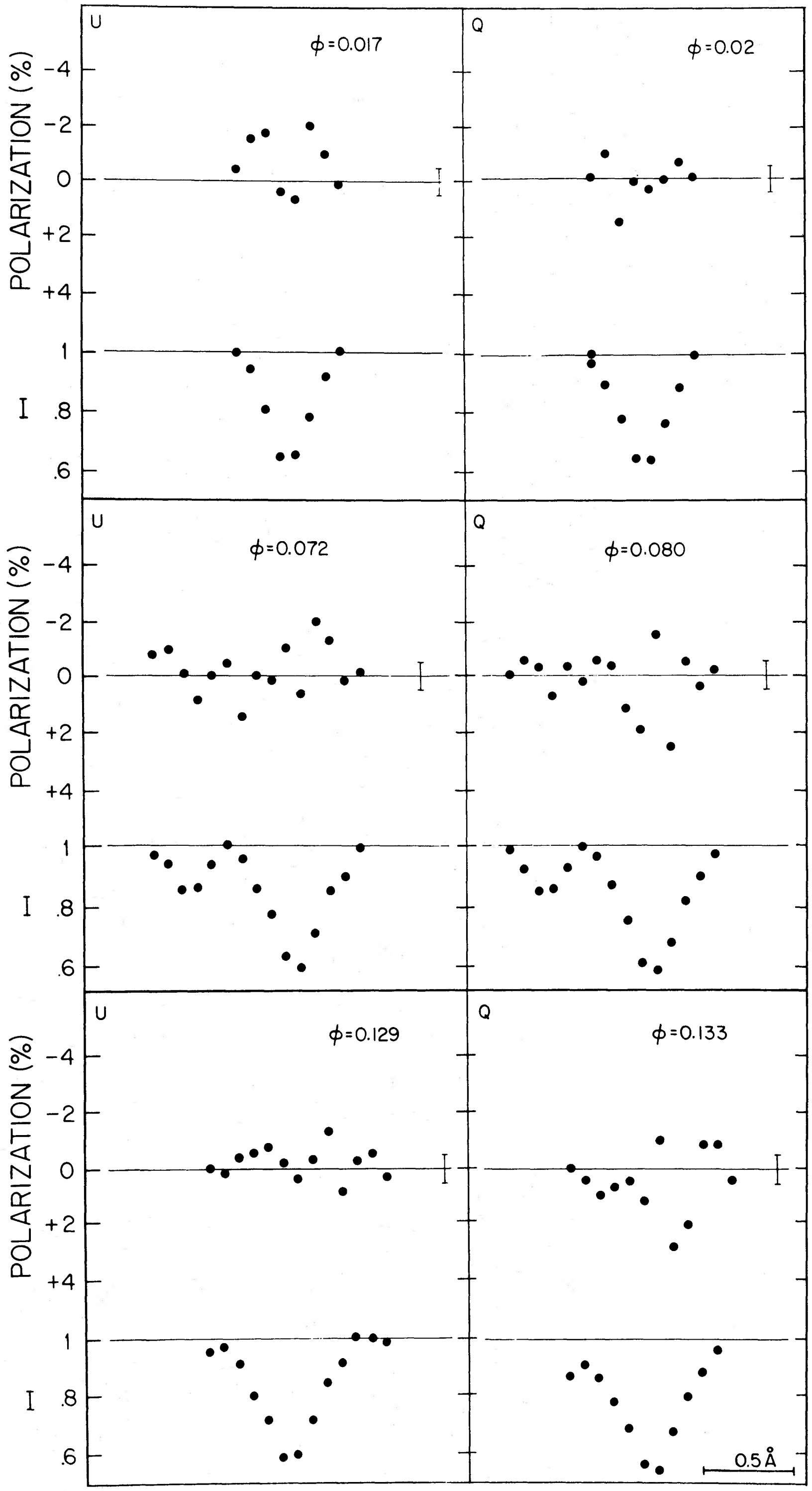

FIG. 9.—The linear polarization and line profiles obtained are shown. The Q and U parameters, measured consecutively on the same night, are shown side by side. Table 3 gives the journal of observation. Wavelength increases to the right.

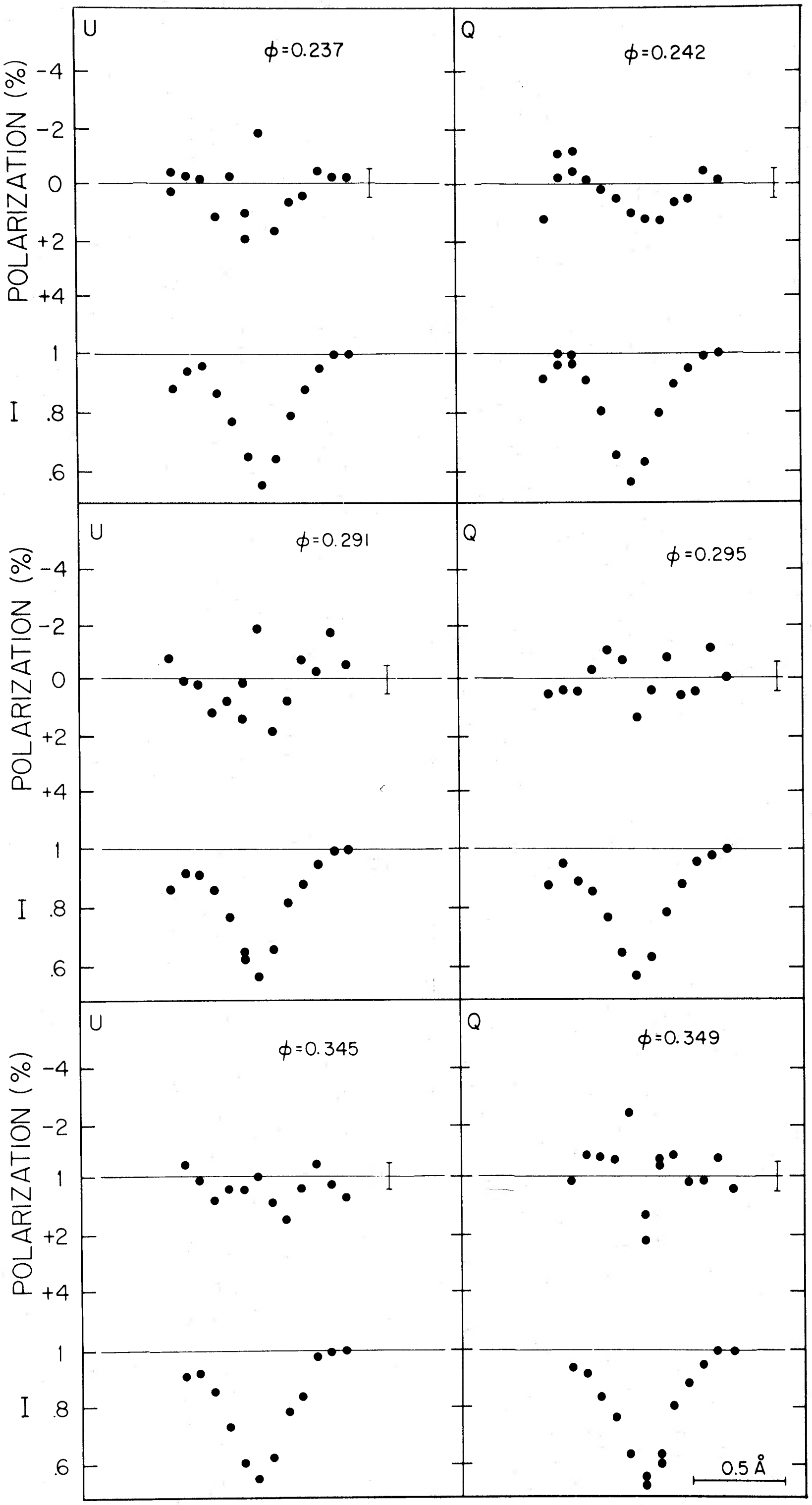

FIG. 10.—Same as Fig. 9

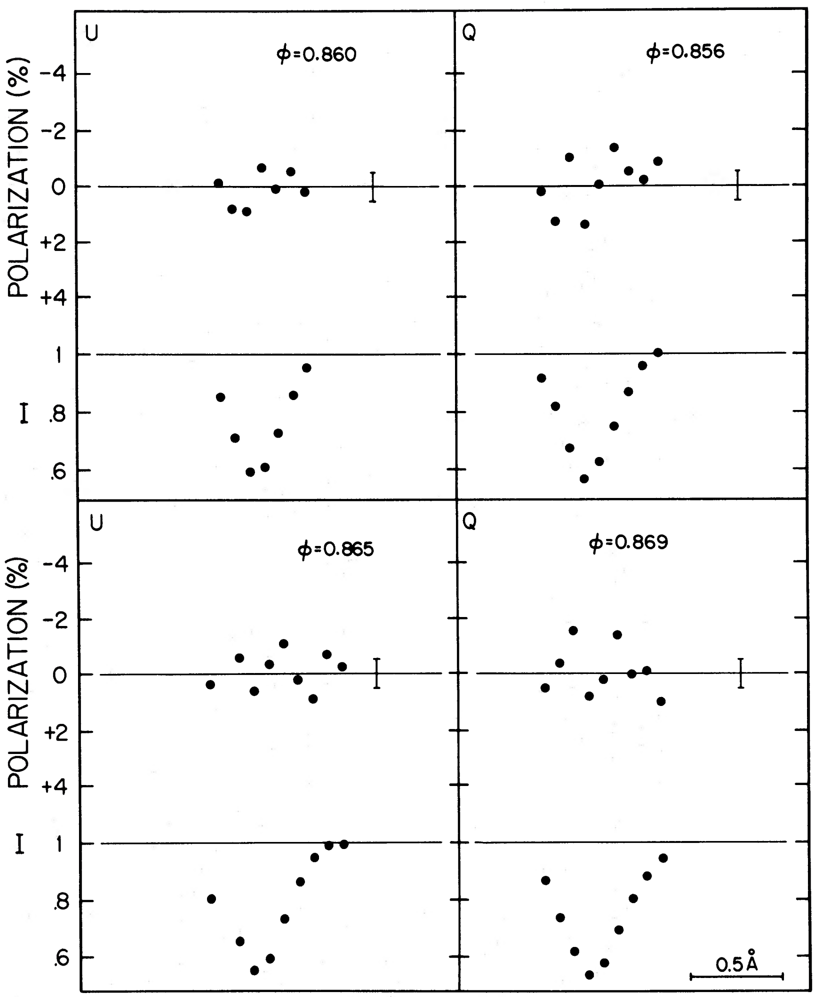

FIG. 11.—Same as Fig. 9

TABLE 3

LINEAR POLARIZATION DATA: JULIAN DATES AND PHASES AT MIDPOINT OF OBSERVATION

JD 2440000+	Phase (U)	Phase (Q)
2259.67	0.017	...
2259.72	...	0.020
2223.77	0.76	...
2223.84	...	0.80
2224.76	0.129	...
2224.83	...	0.133
2226.76	0.237	...
2226.84	...	0.242
2227.75	0.291	...
2227.83	...	0.295
2228.75	0.345	...
2228.83	...	0.349
2255.70	0.803	...
2255.78	...	0.807
2256.69	...	0.856
2256.76	0.860	...
2182.90	0.865	...
2182.97	...	0.869

dependence of the Stokes parameters across spectral lines. Our purpose is to study the circular and linear polarization induced by the Zeeman effect (Zeeman signatures) across the spectral lines of magnetic stars. Our observations reproduce well and appear to be photon-noise–limited. Systematic errors in the polarimeter are considered and shown to be small.

In this first paper of a series, we present the Zeeman signatures and intensity profiles, taken throughout the magnetic cycle, in β CrB. Two lines are observed (Fe II λ4520.2 and Sm II λ4519.6) with a 0.086 Å resolution and discrete sampling. The Zeeman signatures allow us to draw inferences about the magnetic geometry of β CrB: although it may be approximated by a decentered dipole, there are indications that the actual geometry is not cylindrically symmetric (unlike a decentered dipole). More detailed interpretations of our results will follow from model fitting currently in progress.

We have obtained longitudinal magnetic fields from our data by using two different methods. Although the two separate magnetic curves so obtained generally agree with each other and with the published photographic magnetic curves, there are some differences, especially at south polarity. At this stage we can only speculate on the reasons for these differences. We are awaiting the analysis of data obtained for other Ap stars (to be published separately) before drawing conclusions.

The discussions of instrumentation and errors in the polarimetry have been in great part derived from a Ph.D. thesis (Borra 1972) at the University of Western Ontario. One of us (E. F. B.) wishes to thank the Carnegie Institution of Washington for the support of a Postdoctoral Fellowship during much of this investigation. Part of this research has been supported by the National Research Council of Canada.

APPENDIX

DERIVATION OF THE FIRST FORMULA USED TO COMPUTE THE AVERAGE LONGITUDINAL FIELD H_e FROM THE DATA

The separation between the left $r_L(\lambda)$ and right $r_R(\lambda)$ circularly polarized components of the depression profiles of an absorption line formed in the presence of a magnetic field is given by

$$2\Delta\lambda = \frac{\int \lambda r_L(\lambda) d\lambda}{\int r_L(\lambda) d\lambda} - \frac{\int \lambda r_R(\lambda) d\lambda}{\int r_R(\lambda) d\lambda} . \tag{A1}$$

It can be shown (Unno 1956) that

$$r_L(\lambda) = r_I(\lambda) - r_V(\lambda) \quad \text{and} \quad r_R(\lambda) = r_I(\lambda) + r_V(\lambda) , \tag{A2}$$

where $r_V(\lambda) = -V_c(\lambda)$ is the fractional circular polarization expressed in units of the stellar continuum and $r_I(\lambda)$ the unpolarized depression profile. Note that in our figures we display the percentage polarization $V(\lambda)$ in units of the intensity at the wavelength observed. We have, therefore,

$$V_c(\lambda) = \frac{V(\lambda) I(\lambda)}{I_c} \times 10^{-2} , \tag{A3}$$

where I_c is the intensity on the continuum.

We can now write that

$$2\Delta\lambda = \frac{\int \lambda[r_I(\lambda) + V_c(\lambda)] d\lambda}{\int r_L(\lambda) d\lambda} - \frac{\int \lambda[r_I(\lambda) - V_c(\lambda)] d\lambda}{\int r_R(\lambda) d\lambda} . \tag{A4}$$

In the Zeeman effect the equivalent widths in left circularly polarized light, right circularly polarized light, and unpolarized light are equal, and therefore

$$\int r_L(\lambda) d\lambda = \int r_R(\lambda) d\lambda = \int r_I(\lambda) d\lambda . \tag{A5}$$

Hence,

$$\Delta\lambda = \frac{\int \lambda V_c(\lambda) d\lambda}{\int r_I(\lambda) d\lambda} . \tag{A6}$$

REFERENCES

Angel, J. R. P., and Landstreet, J. D. 1970, *Ap. J.* (*Letters*), **160**, L147.
Babcock, H. W. 1953, *Ap. J.*, **118**, 387.
———. 1955, *Carnegie Institution of Washington Yearbook*, **54**, 27.
———. 1958, *Ap. J. Suppl.*, **3**, 141.
———. 1960, in *Stellar Atmospheres*, ed. J. L. Greenstein (Chicago: University of Chicago Press).
———. 1962, in *Astronomical Techniques*, ed. W. A. Hiltner (Chicago: University of Chicago Press), p. 107.
Borra, E. F. 1972, Ph.D. thesis, University of Western Ontario.
———. 1974*a*, *Ap. J.*, **187**, 271.
———. 1974*b*, *Ap. J.*, **188**, 287.
———. 1976, *Pub. A.S.P.*, **88**, 548.
Borra, E. F., and Dworetsky, M. M. 1973, *Ap. J.*, **186**, 211.
Borra, E. F., and Landstreet, J. D. 1973, *Ap. J.* (*Letters*), **185**, L139.
———. 1977, *Ap. J.*, **212**, 141.
Borra, E. F., Landstreet, J. D., and Vaughan, A. H., Jr. 1973, *Ap. J.* (*Letters*), **185**, L145.
Borra, E. F., and Vaughan, A. H. 1976, *Ap. J.* (*Letters*), **210**, L145.
Hale, G. E. 1933, Annual Report to the Director, *Carnegie Institution of Washington Yearbook*.
Hiltner, W. A. 1945, *Ap. J.*, **102**, 438.
Kiepenheuer, K. O. 1953, *Ap. J.*, **117**, 447.
Landstreet, J. D. 1970, *Ap. J.*, **159**, 1001.
Preston, G. W. 1969*a*, *Ap. J.*, **158**, 243.
———. 1969*b*, *Ap. J.*, **158**, 1081.
———. 1971, *Pub. A.S.P.*, **83**, 571.
Preston, G. W., and Pyper, D. M. 1965, *Ap. J.*, **142**, 983.
Preston, G. W., and Sturch, C. 1967, in *The Magnetic and Related Stars*, ed. R. C. Cameron (Baltimore: Mono Book Corp.).
Severny, A. B. 1970, *Ap. J.* (*Letters*), **159**, L73.
Shurcliff, W. A. 1962, in *Polarized Light* (Cambridge: Harvard University Press).
Unno, W. 1956, *Pub. Astr. Soc. Japan*, **8**, 108.
Vaughan, A. H., Jr., and Zirin, H. 1968, *Ap. J.*, **152**, 123.
Wolff, S. C., and Bonsack, W. K. 1972, *Ap. J.*, **176**, 425.
Wolff, S. C., and Wolff, R. C. 1970, *Ap. J.*, **160**, 1049.

Ermanno F. Borra: Département de Physique, Université Laval, Québec, G1K 7P4, Canada

Arthur H. Vaughan: Hale Observatories, 813 Santa Barbara Street, Pasadena, CA 91106